State-independent robust heat-bath algorithmic cooling of nuclear spins

Krishna Shende,[1,*] Arvind,[1,2,†] and Kavita Dorai[1,‡]

[1]*Department of Physical Sciences, Indian Institute of Science Education and Research Mohali,*
Sector 81 SAS Nagar, Manauli, Punjab PO 140306, India
[2]*Punjabi University Patiala, Punjab 147002, India*

In this work we experimentally demonstrate the implementation of a recently proposed robust and state-independent heat-bath algorithmic cooling (HBAC) method [Sadegh Raeisi, Mária Kieferová, and Michele Mosca, Phys. Rev. Lett. **122**, 220501 (2019). doi:10.1103/PhysRevLett.122.220501] on an NMR quantum processor. While HBAC methods improve the purity of a quantum system via iterative unitary entropy compression, they are difficult to implement experimentally since they use sort operations that are different for each iteration. The new robust HBAC method proved that optimal HBAC is possible without prior state information and using a single fixed operation. We modified the protocol to experimentally perform efficient cooling of ^{13}C and ^{15}N spins and provide an optimal decomposition of this modified protocol in terms of quantum gates. We examined the relaxation dynamics of these algorithmically cooled spins, in order to ascertain the effect of decoherence on the cooled states.

I. INTRODUCTION

Quantum computers have the potential to increase the speed and efficiency of certain computational algorithms and simulations [1–3]. However, physical realizations of quantum computers have proved challenging, since sensitive quantum-mechanical effects are easily overwhelmed by thermal fluctuations, and small errors during the implementation of quantum operations are detrimental to their efficient implementation [4]. Protocols such as quantum error correction and fault-tolerant computation were developed to curb these errors, which require the supply of pure qubits throughout the computation process [5]. Enhancing the purity of qubits is important in quantum technologies such as nuclear magnetic resonance (NMR) which have low initial spin polarizations and hence low signal-to-noise ratios.

NMR quantum processors use ensembles of nuclear spins to perform quantum-computational tasks and have the advantages of long qubit decoherence times and optimal gate implementation via high-precision rf pulses [6–8]. Nuclear spins at room temperature are in Boltzmann equilibrium, and such a highly mixed ensemble is a major disadvantage for quantum computation, which requires initial pure states [9]. The population difference between the $|0\rangle$ and $|1\rangle$ states of an NMR qubit is termed the "spin polarization" (ϵ) and at thermal equilibrium

$$\epsilon = P_{|0\rangle} - P_{|1\rangle} = \tanh\left(\frac{\Delta E}{2k_B T}\right) \approx \frac{\hbar\gamma B_z}{2k_B T}, \quad (1)$$

where γ is the gyromagnetic ratio, B_z is the intensity of the external Zeeman magnetic field, k_B is the Boltzmann constant, T is the temperature of the bath, and ΔE is the energy gap between the two states. While the equality on the left-hand side of the above equation is generally true, the approximation on the right-hand side holds under conditions of high temperature (low polarization) as compared to the energy gap. The spin temperature is defined as $T_{\text{spin}} = \hbar\gamma B_z/2k_B\epsilon$, and spins with a polarization higher than their room-temperature polarization can be considered to be "cooled down." Cooling of nuclear spins is hence equivalent to increasing their polarization, which is limited by the Shannon bound [10] for a closed quantum system. It is therefore imperative to devise methods for the cooling of nuclear spins.

The NMR quantum information processor has been termed as a system having "good dynamics versus bad kinematics" [11]. To improve this situation, we need to prepare the initial state of the NMR quantum information processor such that a large number of spins in the ensemble are in the same quantum state. One way to prepare an ensemble of spins in a pure state is to cool the entire system down to very low temperatures, but this is not feasible with the current technology. Other spin-cooling proposals include algorithmic cooling [12–17], dynamic nuclear polarization [18], parahydrogen-induced polarization [19],

* ph19032@iisermohali.ac.in
† arvind@iisermohali.ac.in
‡ kavita@iisermohali.ac.in

and optical pumping [20], all of which have met with varying degrees of success. Of all these cooling methods, algorithmic cooling (AC) has shown the greatest promise for applications to quantum computing.

Algorithmic cooling was introduced by Schulman [12] to increase the polarization of selected qubits in a closed system. The protocol uses additional ancilla qubits which are called reset qubits, and the combined system and reset qubits are subjected to an overall unitary transformation such that the system qubits move toward a state with lower entropy/increased purity and hence with a lower spin temperature, while the reset qubits heat up and gain entropy. The major disadvantage of the AC protocol is that for spins at room temperature, the number of spins required to cool the target spin is very large (typically of the order of 10^{12} spins). This obstacle was circumvented by Boykin [13] in an extension to AC, called heat-bath algorithmic cooling (HBAC), in which a contact between the heat bath and the system is introduced, which pumps the excess entropy out of the system into the heat bath [21,22]. Later, an extension to the HBAC method was proposed, called the partner pairing algorithm (PPA), which sorts the diagonal elements of a density matrix for entropy compression, and it was proved that this sort operation is an optimal entropy compression step for HBAC [23]. If the decoherence time of the reset qubits is significantly less than that of the computational qubits, it is possible to iteratively achieve cooling of the target qubits. However, despite repetitive cooling, the target qubits cannot be fully purified, and a limit of purification was computed [24–26]. The role of non-Markovian processes in improving cooling efficiency was explored and several protocols were suggested to optimize the thermalization strategy [27]. It was discovered that the unitarity of the compression operation limits the cooling of HBAC techniques [28]. It was recently demonstrated that the cooling limit of HBAC protocols can be enhanced in the presence of noise [29]. The overall rationale behind all these methods is to perform various unitary transformations on a multi-spin system where a part of the system moves toward a higher polarization (lower entropy) and hence lower effective spin temperature, at the cost of the other part which heats up, and in some of the methods this heat is transported away by another set of transformations.

On NMR quantum processors, various experiments based on the HBAC protocol have been performed [30–38]. Several iterations of HBAC was performed on three solid-state NMR qubits in order to cool a single qubit [39]. The PPA-HBAC algorithm was used to implement a quantum Otto heat engine with greater thermal efficiency than traditional engines [40]. An HBAC method using correlated spin-bath interactions was devised which uses spin-spin cross-relaxation (the nuclear Overhauser effect) to achieve higher polarization enhancement than the PPA-HBAC method [41]. Recently, HBAC has been used

to enhance spin polarization in nitrogen-vacancy center quantum devices [42,43].

All the previous experimental implementations of HBAC achieved cooling via the PPA-HBAC method, which requires a different compression unitary to be implemented as well as knowledge of the state of the system in every iteration. Raeisi's state-independent HBAC technique [44], called the two-sort algorithmic cooling (TSAC) technique, proposed a new fixed operation to achieve algorithmic cooling that does not require any prior knowledge of the state. We note here that the compression unitary used for the three-qubit system is the same for every cooling iteration. In the PPA-HBAC method, one has to use a state-specific compression unitary for systems with more than three qubits. The real advantage of the TSAC-HBAC method becomes apparent for systems with more than three qubits, where this method uses a single fixed compression unitary for every iteration. The work done in this paper is a realization of the TSAC method on an NMR quantum processor. We experimentally demonstrate the successful implementation of this protocol on two different three-qubit NMR systems: the first system having a ^{13}C spin as the target qubit to be cooled, and the second system having a ^{15}N spin as the target qubit to be cooled. We were able to achieve large polarization enhancements and concomitantly were able to decrease the corresponding spin temperatures of the target spins to well below room temperature. The original theoretical proposal decomposed the fixed unitary compression operator in terms of shift operators, which were further decomposed in terms of the quantum Fourier transform (QFT), the inverse QFT, and single-qubit rotation gates. The QFT is a resource-intensive operation whose circuit depth increases tremendously with the number of qubits, which makes it more vulnerable to experimental errors [45]. We therefore designed an optimal decomposition of the shift operators in terms of standard multiqubit gates such as Toffoli, CNOT, and NOT gates, which makes it easier to experimentally implement the circuit. After implementing several cycles of TSAC, we were able to enhance the polarization of the ^{13}C and ^{15}N spins by 4.3 and 5.95 times respectively, as compared to their thermal equilibrium polarizations, which translates to cooling their spin temperatures down to about 71 K and 51 K, respectively. It is noteworthy that ^{15}N spins (due to their low gyromagnetic ratio) have very low spin polarizations at thermal equilibrium (approximately one-tenth that of ^{1}H spins), and we were able to considerably enhance their polarization via the state-independent HBAC protocol. Further, we studied the relaxation dynamics of the algorithmically cooled spins by measuring their T_1 and T_2 relaxation rates and observed that algorithmically cooled states relax in a way similar to thermal states, thus retaining the good dynamics of the NMR spin system.

This paper is organized as follows. The standard HBAC and PPA-HBAC protocols are described in Sec. II A, while

the state-independent TSAC protocol is given in Sec. II B. The optimal circuit decomposition of the compression unitary is described in Sec. II C. The experimental implementation of the state-independent HBAC protocol is presented in Sec. III. Section III A contains experimental details, whereas Secs. III B and III C describe the results of experimentally cooling a ^{13}C-labeled and a ^{13}C-^{15}N-labeled system, respectively. Section IV contains a few concluding remarks.

II. THEORETICAL FRAMEWORK

A. Standard heat-bath algorithmic cooling protocols

The AC scheme exploits the fact that cooling of specific spins below their equilibrium polarization can be achieved by using a reversible unitary operation to increase the polarization of the target spins, relative to the rest of the spins. Closed system AC executes an entropy compression operation on spins which are initially at thermal equilibrium, creating a difference in the spin temperatures of the spins such that the reset spins heat up and the computational spins cool down, as represented by [12]

$$\rho \xrightarrow{\text{Compression}} \rho' = U\rho U^\dagger. \tag{2}$$

The reset qubits can be assumed to have an "average" polarization (denoted by ϵ_r) and if ϵ_i and ϵ_c represent the initial polarization and the polarization of the computational qubit, respectively, in general $\epsilon_c > \epsilon_i > \epsilon_r$ after entropy compression. The density matrix of the computational spin is obtained by taking a trace over the $n-1$ reset spins $\rho_{\epsilon_c} = \text{Tr}_{n-1}(\rho')$. The AC method is a closed-cycle method where cooling is limited by the Shannon bound for information compression [10,46].

An upper bound on spin cooling for closed system AC, called the Shannon bound, can be derived by interpreting the spin state in terms of information theory, such that the information content (IC) of the spin is defined using Shannon entropy H, and the relation between spin polarization (ϵ) and IC is given by [16,33]

$$H_{1\text{qubit}} = -\left[\frac{1-\epsilon}{2}\ln\left(\frac{1-\epsilon}{2}\right) + \frac{1+\epsilon}{2}\ln\left(\frac{1+\epsilon}{2}\right)\right],$$

$$IC_{1\text{qubit}} = 1 - H_{1\text{qubit}} = \frac{\epsilon^2}{\ln 4} + O(\epsilon^4). \tag{3}$$

It is to be noted that the Shannon bound given above is a theoretical upper limit for closed systems and is used in the rest of this paper as a useful reference bound. It is not to be equated with the maximum achievable polarization.

Cooling in the AC scheme can be enhanced by incorporating a contact between a heat bath and the system. The excessive heat in the reset spins is then pumped out of the system into a heat bath, where it is removed and the spins are cooled to the bath temperature, a step called the "reset" step [13]. The system spins are categorized as a target spin (which is to be cooled), a set of scratch spins (which can either be a higher-dimensional qudit or a string of qubits) which help in entropy compression, and a set of m reset spins which are brought into contact with the heat bath [26]. The target and scratch spins together are referred to as the computational spins. The entire process of entropy compression and the reset step is known as heat-bath algorithmic cooling [21,22]. The HBAC method works optimally if the ratio R between the thermalization times (T_1) of computational to reset spins satisfies $R \gg 1$, so that several cooling cycles can be implemented, and the state of the computational spins remains unchanged during the reset process. The reset step amounts to tracing over the reset spins and replacing them with heat-bath spins. It is assumed that the heat-bath capacity is so large that the spin-bath interaction has no effect on the bath temperature.

The HBAC method was further optimized in a method called the partner pairing algorithm [23], where in each iteration the diagonal elements of the density matrix are sorted in decreasing order. It is to be noted that the sort operations and their complexity keep changing from iteration to iteration.

The steps of the PPA-HBAC algorithm can be written as

$$\rho \xrightarrow{C} \rho' = U_K \rho U_K^\dagger.$$
$$\rho' \xrightarrow{R} \rho'' = \text{Tr}_m\left[\mathcal{L}(\rho' \otimes \rho_{\epsilon_b}^{\otimes m})\right]. \tag{4}$$

The first step in the PPA-HBAC protocol is "compression," which achieves a temperature gradient between the system and reset qubits, raising the entropy of one part of the system, while lowering it for the other part, which is achieved by the unitary operation U_K. This temperature gradient can be further maximized by sorting the density matrix elements in descending order, using the compression unitary U_K. $\mathcal{L}$ represents nonunitary evolution during the period in which the reset qubits cool down due to interaction with the heat bath; ρ_{ϵ_b} represents the state of the bath spin and ϵ_b is the heat-bath polarization. It is to be noted that in the second line of Eq. (4), we first take a tensor product of ρ' with the bath qubits, then apply a nonunitary operator $\mathcal{L}$, and finally trace over the m bath qubits, obtaining ρ'' as the density operator for the system qubits, which has the same dimensionality as that of the density operators ρ and ρ'. The cooling limit is achieved once no more entropy extraction is possible, that is, when system state reaches a steady state which is not changed by compression and refresh [$\rho = \rho''$ in Eq. (4)].

The cooling limit depends on the number of reset qubits and the total number of qubits in the spin system. For an n-spin system and only a single (or two) reset qubit(s), the PPA-HBAC cooling limit (i.e., the maximum achievable

polarization) is computed to be [26]

$$\epsilon_{\max} = \frac{(1 + \epsilon_b)^{2^{n-2}} - (1 - \epsilon_b)^{2^{n-2}}}{(1 + \epsilon_b)^{2^{n-2}} + (1 - \epsilon_b)^{2^{n-2}}}. \tag{5}$$

A major limitation of the PPA algorithm is that in each iteration, complete information about the state of the system is needed in order to set up the sort operation. In a domino effect, this in turn implies that the PPA compression operation also changes after every iteration, which makes the PPA-HBAC method experimentally challenging to implement.

A schematic of the PPA-HBAC method is given in Fig. 1(a) in which an entropy compression operation is first implemented which arranges the diagonal elements of the density matrix in decreasing order. These sort operations are state dependent and hence the unitaries used in each compression step of the PPA-HBAC method are different. The excess heat of the reset spins is pumped out of the system by making them interact with the heat bath.

B. Two-sort algorithmic cooling

An HBAC method was recently proposed (termed the two-sort algorithmic cooling (TSAC) method) which achieves optimal cooling of the system spins, and has been shown to be better than the PPA-HBAC method in terms of circuit complexity and robustness against noise [44]. Optimality in this context implies achieving the same final cooling as the PPA-HBAC method, with less circuit complexity, albeit with a larger number of cooling rounds. Cooling is achieved by recursively operating a fixed unitary matrix followed by the reset step, without requiring prior state information. The general unitary matrix for n spins (U_{TS}^n) is given by

$$U_{\text{TS}}^n = \begin{bmatrix} 1 & & & & & \\ & X & & & & \\ & & \cdot & & & \\ & & & \cdot & & \\ & & & & \cdot & \\ & & & & X & \\ & & & & & 1 \end{bmatrix} \tag{6}$$

where X denotes the Pauli σ_x matrix. Unlike the unitary compression operator in the PPA algorithm which achieves a descending sort of the diagonal elements, the two-sort unitary U_{TS}^n swaps every two neighboring diagonal elements, except for the first and last elements. The matrix is $2^n \times 2^n$ and acts on the computation and reset spins, achieving a local partial sort of the density matrix diagonal elements.
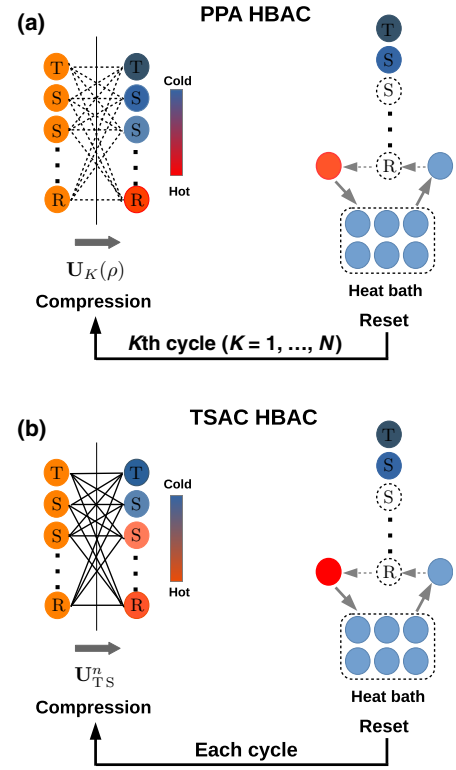

FIG. 1. Schematic to illustrate the different steps of the PPA-HBAC and state-independent HBAC protocols. The n-spin system is categorized as target spins (labeled T), scratch spins (labeled S) and reset spins (labeled R). Temperature is color-coded, with shades of blue indicating cooling and shades of orange to red indicating heating. (a) During every iteration in the PPA-HBAC method, the compression unitary U_K extracts entropy from the target spin and redistributes it among the reset spins, such that the target spin cools down and the reset spins heat up. The compression step is followed by a reset step, where the hot reset spins are brought into contact with the heat bath. The compression unitary $U_K(\rho)$ depends on the state ρ and changes after every cooling cycle, where $K = 1, 2, \ldots, N$ denotes the number of the current cooling cycle. (b) Only a fixed compression unitary U_{TS}^n for an n-qubit system is required in the state-independent TSAC HBAC method to redistribute entropy and develop a temperature gradient among spins. The compression step is followed by a reset step where the reset spins equilibrate with the surrounding heat bath. The dotted lines in (a),(b) indicate redistribution of entropy among the system spins to create a temperature gradient.

For three spins, the unitary compression operator is given by

$$U_{\text{TS}}^3 = \begin{bmatrix} 1 & 0 & 0 & 0 & 0 & 0 & 0 & 0 \\ 0 & 0 & 1 & 0 & 0 & 0 & 0 & 0 \\ 0 & 1 & 0 & 0 & 0 & 0 & 0 & 0 \\ 0 & 0 & 0 & 0 & 1 & 0 & 0 & 0 \\ 0 & 0 & 0 & 1 & 0 & 0 & 0 & 0 \\ 0 & 0 & 0 & 0 & 0 & 0 & 1 & 0 \\ 0 & 0 & 0 & 0 & 0 & 1 & 0 & 0 \\ 0 & 0 & 0 & 0 & 0 & 0 & 0 & 1 \end{bmatrix}. \tag{7}$$

The polarization of spins depends on the values of the diagonal elements of the density matrix of the system. The unitary matrix U_{TS}^n [Eq. (6)] keeps the first and the last diagonal element of the density matrix unchanged, and exchanges the position of the other elements with their immediate neighbors. By choosing a spin with low polarization as the first spin, and performing U_{TS}^n iteratively on a system in thermal equilibrium, the polarization of the first spin can be substantially enhanced.

A schematic diagram of the TSAC HBAC method is given in Fig. 1(b), where a single unitary U_{TS}^n is used to compress entropy among n spins, thereby creating a temperature gradient between the system spins. The target spin is cooled while the reset spins are heated up. The reset step is the same for the PPA-HBAC and the TSAC HBAC protocols. The reset step is repeated several times to thermalize the reset spins to the heat-bath temperature. We note here that for three qubits, the final polarization achieved by both the PPA-HBAC and TSAC methods is the same, although the TSAC method has a reduced circuit complexity and is easier to implement experimentally. However, the TSAC method requires more iterations to reach the saturation polarization. The real advantage of the TSAC method becomes evident for systems with more than three qubits, where the same unitary is applied in every iteration, as opposed to the PPA-HBAC method which requires the design of a different unitary for each iteration.

In the low-polarization limit, the spin temperature is inversely proportional to the polarization and can be computed from

$$T_1.\epsilon_1 = T_2.\epsilon_2, \tag{8}$$

where T_1, T_2 are the initial and final spin temperatures and ϵ_1, ϵ_2 are the initial and final spin polarizations, respectively. At thermal equilibrium, the initial polarization values of the ^{1}H, ^{13}C, and ^{15}N spins are approximately 48.14×10^{-6}, 12.1×10^{-6}, and 4.88×10^{-6}, respectively. For each of the molecules used in this study, the initial polarization value of the ^{1}H spin is set to 1.0 and the polarization values of all other spins are quoted relative to it.

C. Optimal circuit decomposition of the compression unitary

The first and last elements of the diagonal of the U_{TS}^n unitary operator (the 1×1 blocks in the top left and bottom right corners of the matrix) in Eq. (6) correspond to SHIFT$_m$ operators which shift the spin state m times to the right or the left. This can be achieved by applying a multiple-control Toffoli gate (which is a controlled-controlled NOT with one target and $n-1$ controls) followed by a NOT gate on the last spin. The suggested

decomposition in Raeisi *et al.* [44] for these SHIFT operators is a QFT and an inverse QFT, sandwiching a set of rotation operators of specific rotation angles and phases.

In order to use fewer experimental resources and alleviate the detrimental effects of noise during long gate implementation times, we have decomposed the SHIFT operator into a sequence of a three-qubit Toffoli gate, a two-qubit CNOT gate, and a single-qubit NOT gate. The complexity of the circuit has been further reduced by using an approximate Toffoli gate as described in Ref. [47], which differs from the actual Toffoli gate by a phase of one of its amplitudes (the phase of the $|101\rangle$ state is reversed). It is to be noted that the circuit decomposition we have employed achieves the same final cooling as the original TSAC protocol; however, the unitary decomposition is easier to implement experimentally. The final compression unitary operator which has been experimentally implemented is given by

$$U'_{TS} = \begin{bmatrix} 1 & 0 & 0 & 0 & 0 & 0 & 0 & 0 \\ 0 & 0 & 1 & 0 & 0 & 0 & 0 & 0 \\ 0 & 1 & 0 & 0 & 0 & 0 & 0 & 0 \\ 0 & 0 & 0 & 0 & 1 & 0 & 0 & 0 \\ 0 & 0 & 0 & 1 & 0 & 0 & 0 & 0 \\ 0 & 0 & 0 & 0 & 0 & 0 & -1 & 0 \\ 0 & 0 & 0 & 0 & 0 & 1 & 0 & 0 \\ 0 & 0 & 0 & 0 & 0 & 0 & 0 & 1 \end{bmatrix}. \tag{9}$$

The negative sign in the $|101\rangle\langle110|$ position has no effect on the TSAC protocol and the results remain the same.

The complete quantum circuit for implementing the TSAC protocol is depicted in Fig. 2(a), for a three-qubit system initially prepared in a thermal equilibrium state. The circuit inside the green box is the general compression unitary U'_{TS}, as given in Eq. (9). This unitary is decomposed as a sequence of a right SHIFT operator, a left SHIFT operator, a Toffoli gate, and a NOT gate, enclosed in the blue dashed box, the red dashed box, the magenta shaded box, and the unfilled box, respectively, in Fig. 2(a). Each SHIFT operator is further decomposed as a Toffoli gate, a CNOT gate, and a NOT gate given in the orange shaded, yellow shaded, and unfilled boxes, respectively. The reset step of the TSAC algorithm is denoted by the indigo shaded box, with the horizontal lines depicting the heat bath. Figures 2(b)–2(e) depict the NMR pulse sequences for a NOT, a CNOT, and a Toffoli gate, respectively.

III. EXPERIMENTAL IMPLEMENTATION

A. Experimental details

All experiments were performed at ambient temperature (303 K) on a Bruker Avance III 600-MHz NMR spectrometer equipped with a standard 5-mm TXI probe.
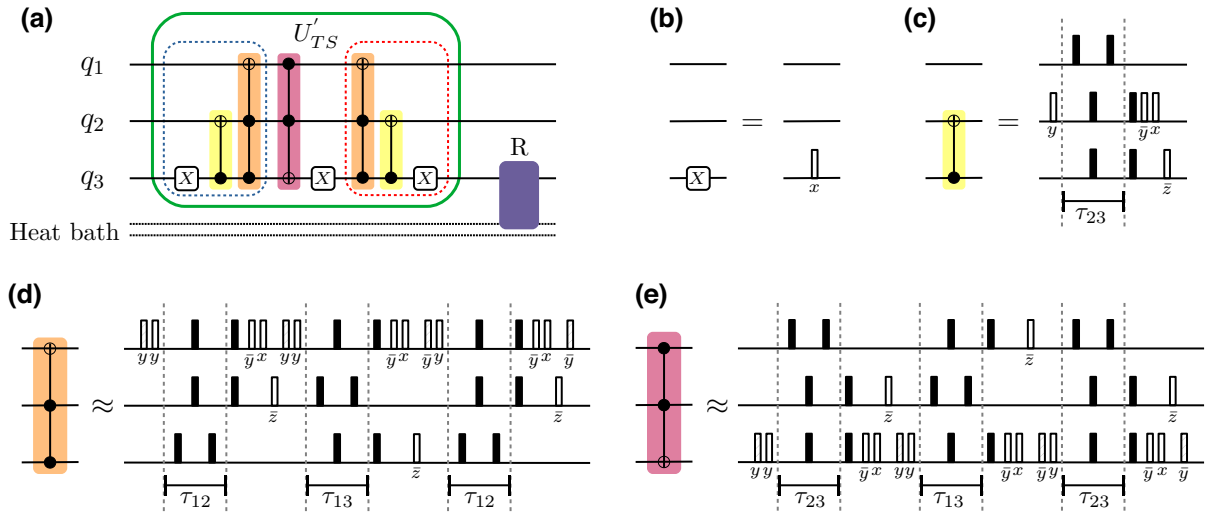
FIG. 2. (a) Schematic of the quantum circuit to implement a single cycle of the state-independent HBAC protocol on a three-qubit system, with q_i labeling the qubit. The green box encloses the entire compression unitary operator, while the dashed blue and red boxes enclose the circuits corresponding to the right shift and the left shift operator, respectively; R denotes the reset operation. The NMR pulse sequence corresponding to the implementation of (b) a NOT gate, (c) a CNOT gate, (d) a Toffoli gate with the target being the first qubit, and (e) a Toffoli gate with the target being the third qubit, respectively. The black, unfilled and cross-hatched rectangles represent π, $\pi/2$, and $\pi/4$ spin-selective rf pulses, respectively. The phase of the pulse is written below the respective pulse, with a bar over a phase denoting negative phase; the delays are denoted by $\tau_{ij} = 1/2J_{ij}$, where i, j are the qubit labels and J_{ij} is the strength of the scalar coupling.

The Hamiltonian for a three-spin system in the rotating frame, assuming a high-temperature and high-field approximation, is given by [48]

$$\mathcal{H} = -\hbar \sum_{i=1}^{3} \omega_i I_z^i + \hbar \sum_{i<j=1}^{3} J_{ij} I_z^i I_z^j, \qquad (10)$$

where ω_i, I_z^i represent the offset frequency and the z-component of the spin angular momentum of the ith spin respectively, and J_{ij} is the strength of the scalar coupling between the ith and jth spins.

The TSAC cooling protocol was experimentally implemented on two molecules. The first molecule was $^{13}C_2$-labeled glycine with both the $^{13}C_1$ spin being the target spin to be cooled and the ^1H spin being the reset spin [see Fig. 3(a) for the molecular structure, chemical shifts ν_i, and scalar coupling values J_{ij}]. The glycine molecule was dissolved in D_2O and a paramagnetic reagent $Cr(acac)_3$ was added to improve the T_1 ratio between the target and reset nuclei. This molecule is an example of an A_2XX' spin system, with two equivalent ^1H spins (A_2) and two magnetically inequivalent ^{13}C spins (XX'). The second molecule was ^{13}C-^{15}N-labeled formamide, with both the ^{15}N and the ^{13}C spins being the targets to be cooled, and the ^1H spin being the reset spin [see Fig. 4(a) for the molecular structure, chemical shifts ν_i. and scalar coupling values J_{ij}]. Each single-qubit rotation gate was implemented using spin-selective rf pulses of appropriate phase, power, and time duration, while two-qubit and three-qubit

gates were implemented via evolution under the system Hamiltonian using time delays interspersed with π pulses to refocus chemical shifts and retain only the desired scalar coupling interactions. More experimental details of NMR pulse sequences for various quantum gates used in this work can be found in Refs. [49–51]. On the TXI probe, the duration of the $\Pi/2$ pulses for ^{15}N, ^{13}C, and ^1H were 38 μs at a power level of 246.6 W, 12.95 μs at a power level of 237.3 W, and 7.3 μs at a power level of 19.9 W, respectively. Gradient ascent pulse engineering (GRAPE), an optimal control algorithm, was used to generate high-fidelity rf pulses of duration approximately 150 μs to implement single-qubit rotations on the $^{13}C_2$-labeled glycine system. The total time taken to implement the compression unitary on the $^{13}C_2$-labeled glycine system and on the ^{13}C-^{15}N-labeled formamide system was 0.302 s and 0.23 s respectively, which is much shorter than the relaxation times of all the spins in both systems.

B. Experimentally cooling the ^{13}C spin

Most previous experimental algorithmic cooling protocols have focused on cooling ^{13}C spins, due to their small gyromagnetic ratios and correspondingly low initial polarization at thermal equilibrium (approximately one-fourth that of the ^1H spin). We hence chose $^{13}C_1$ as the target spin to be cooled in the $^{13}C_2$-labeled glycine system and the ^1H spin as the reset spin due to its high polarization (set to 1.0) at thermal equilibrium and its fast T_1 relaxation time as compared to the $^{13}C_1$ spin. Interestingly, this system has
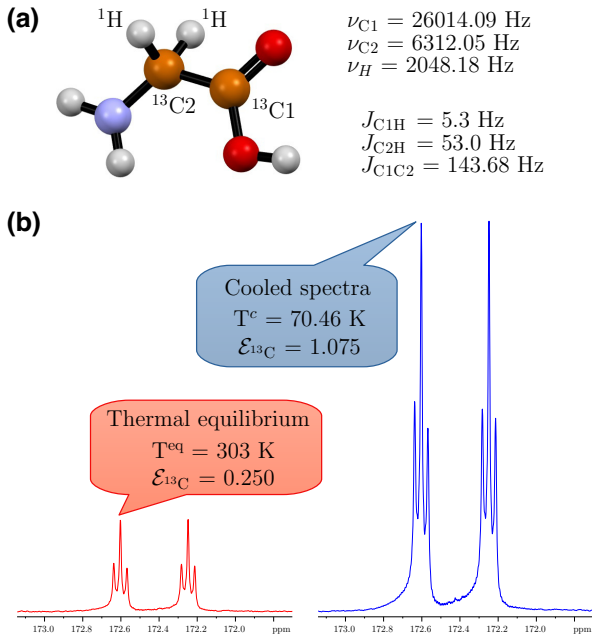
FIG. 3. (a) Molecular structure of $^{13}C_2$-labeled glycine with the $^{13}C_1$, $^{13}C_2$, and ^1H spins, encoded as the first, second, and third qubit, respectively. The offset rotation frequency for each spin and scalar coupling strengths are listed alongside. (b) The ^{13}C spectrum (red) on the left was recorded at thermal equilibrium while the spectrum (blue) on the right is the enhanced polarization spectrum recorded after algorithmic cooling of both the ^{13}C spins. The corresponding polarizations and spin temperatures are annotated.

FIG. 4. (a) Molecular structure of ^{13}C-^{15}N-labeled formamide, with the ^{15}N, ^{13}C, and ^1H spins encoded as the first, second, and third qubit, respectively. The offset rotation frequency for each spin and the scalar coupling strengths J are listed alongside. (b) The ^{15}N NMR spectrum (red) on the left was recorded at thermal equilibrium, while the spectrum (blue) on the right is the enhanced polarization spectrum recorded after algorithmic cooling of the ^{15}N spin. The corresponding polarizations and spin temperatures are annotated.

another $^{13}C_2$ spin, whose polarization also has the potential to be enhanced. However, as will be seen below, due to its unfavorable relaxation properties this spin does not cool down to the same extent as the target spin.

1. Optimizing the TSAC reset delay

We simulated the change in $^{13}C_1$ spin polarization as a function of the reset delay in order to find the optimum reset delay for iterative TSAC cooling. We assumed ideal compression gate implementation and accounted for the decay in the polarization during the reset delay which is governed by

$$\epsilon_t = (\epsilon_{\text{init}} - \epsilon_{\text{eq}}) \exp^{-t/T_1} + \epsilon_{\text{eq}}, \qquad (11)$$

where ϵ_{init} and ϵ_{eq} are the initial and thermal equilibrium spin polarizations, respectively. The reset delay was varied from $0.2T_{1R}$ to $5T_{1R}$, where T_{1R} is the longitudinal relaxation time of the reset qubit, and as can be seen from Fig. 5, maximum $^{13}C_1$ polarization was obtained for a reset delay of 3.14 s, which is approximately $2T_{1R}$. We note here that, when the reset delay time is increased beyond $2T_{1R}$, the target qubit and the scratch qubits no longer remain
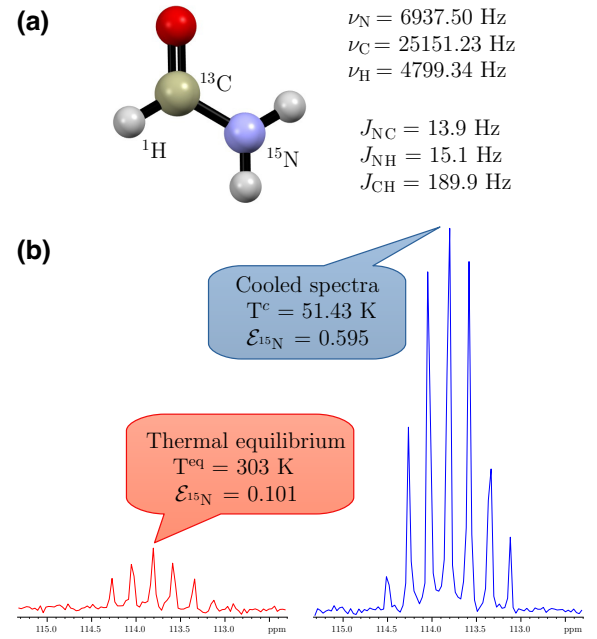
isolated but begin interacting with the bath. The polarization of the target qubit and of the scratch qubits decreases, which leads to a loss of information content in the system. Consequently, the polarization of the $^{13}C_1$ spin is also reduced. We hence set the reset delay time during heat-bath interaction to the optimal value of approximately $2T_{1R}$ in our experiments and performed multiple rounds of TSAC cooling.

2. Spin temperature after several TSAC cycles

The ^{13}C spectra at thermal equilibrium and after implementation of 10 rounds of the TSAC cooling procedure are shown in Fig. 3(b), with "hot" thermal equilibrium spectra shown in red and the algorithmically cooled spectra in blue, plotted to the same scale. The ^{13}C spectra obtained after algorithmic cooling using the TSAC method show a considerable increase in spin polarization (approximately 4.3 times), with peak intensities being much higher than those obtained at thermal equilibrium. This substantial enhancement in the polarization of the ^{13}C spin is attributable to the large difference in the initial polarizations of the ^1H and ^{13}C spins, with the ^1H spin having four times higher polarization than the ^{13}C spin (for more details of the expected polarization enhancement see the
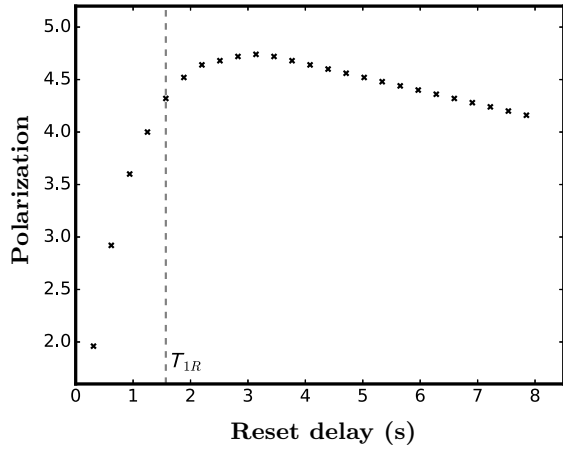
FIG. 5. Simulation of $^{13}C_1$ spin polarization as a function of the TSAC reset delay for the $^{13}C_2$-labeled glycine system; T_{1R} marks the T_1 relaxation time of the ^{1}H reset spin. As the reset delay is increased, the scratch and reset qubits will no longer remain isolated from the decohering bath, which leads to an overall loss in polarization. Hence, a decrease in the target qubit polarization is observed.

calculations in Ref. [33]). The population of an energy level (and hence the polarization bias) is directly proportional to the area under the corresponding resonance peak and was computed via integration. The theoretical value of maximum achievable ^{13}C polarization (Shannon bound) for the $^{13}C_2$-labeled glycine system computed from Eq. (3) is given by

$$IC_{eq} = 17.84 \frac{\epsilon_{C,\,eq}^2}{\ln 4} = \frac{\epsilon_{SB}^2}{\ln 4} \qquad (12)$$
$$\Rightarrow \epsilon_{SB} = 4.224\epsilon_{eq}.$$

After 10 rounds of TSAC cooling, we were able to experimentally achieve a final polarization of approximately 4.3 for the $^{13}C_1$ spin, and were clearly able to surpass the Shannon bound for this system. We note here that the Shannon bound is obeyed only by closed systems and therefore is not expected to be obeyed in the current situation. Hence, the observed violation of the Shannon bound is not unexpected and is used here merely as a point of reference. The final spin temperatures attained by the target $^{13}C_1$ spin, the second $^{13}C_2$ spin, and the reset spin in the $^{13}C_2$-labeled glycine system are tabulated in Table I. It can be seen that the target spin has been substantially cooled down to approximately 71 K. The buildup of $^{13}C_1$ spin polarization after implementation of every cycle of TSAC cooling is shown in Fig. 6, and saturation of the polarization enhancement is attained after four cycles of TSAC cooling. The red curve in Fig. 6 depicts the ideal case of algorithmic cooling without any deviation from U'_{TS}. The actual polarization increase after every cycle after considering the imperfections in the implementation in the TSAC
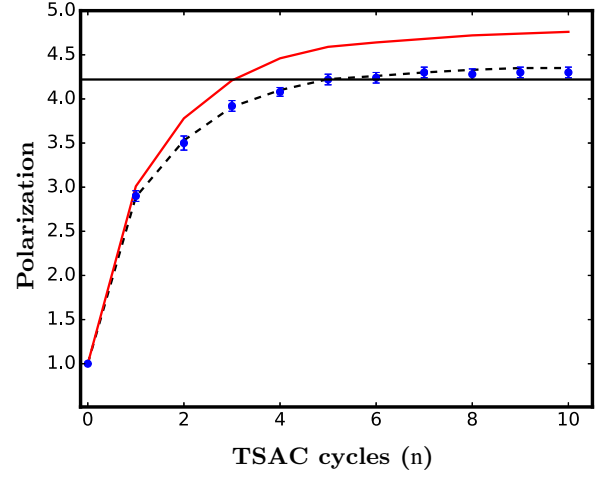

FIG. 6. Polarization of $^{13}C_1$ spin versus number of cycles (n) of TSAC algorithmic cooling implemented on the $^{13}C_2$-labeled glycine system. Theoretically expected and experimentally obtained values are depicted by a black dashed line and blue dots, respectively. The solid black line denotes the Shannon bound for maximum achievable polarization ϵ_{SB} in a closed system. The dotted line denotes the theoretical prediction of the polarization enhancement, taking into account the actual gate fidelities and reset delays. The red solid curve is the polarization enhancement considering the ideal TSAC protocol for the $^{13}C_2$-labeled glycine system.

protocol is depicted by the black dashed curve. We have observed that U'_{TS} is implemented with 0.96 efficiency for the $^{13}C_2$-labeled glycine system.

3. Magnetization trajectories during compression unitary implementation

The plots of individual spin magnetizations of the $^{13}C_2$-labeled glycine system at the end of implementation of each gate in the quantum circuit of the TSAC algorithm are shown in Fig. 7(a). The way entropy compression proceeds after each gate can be visualized from these magnetization plots, with the magnetization being plotted on the y axis, and the gate number being denoted along the x axis; gate number 1, 2, 3, 4, 5, 6, 7, and 8 corresponds to a NOT,

TABLE I. Initial and final spin polarizations (ϵ_1, ϵ_2) and final spin temperature [T(K)] attained by each spin in the three-spin $^{13}C_2$-labeled glycine system after 10 rounds of algorithmic cooling. All polarization values are given relative to the initial polarization of the ^{1}H spin, which is set to 1.

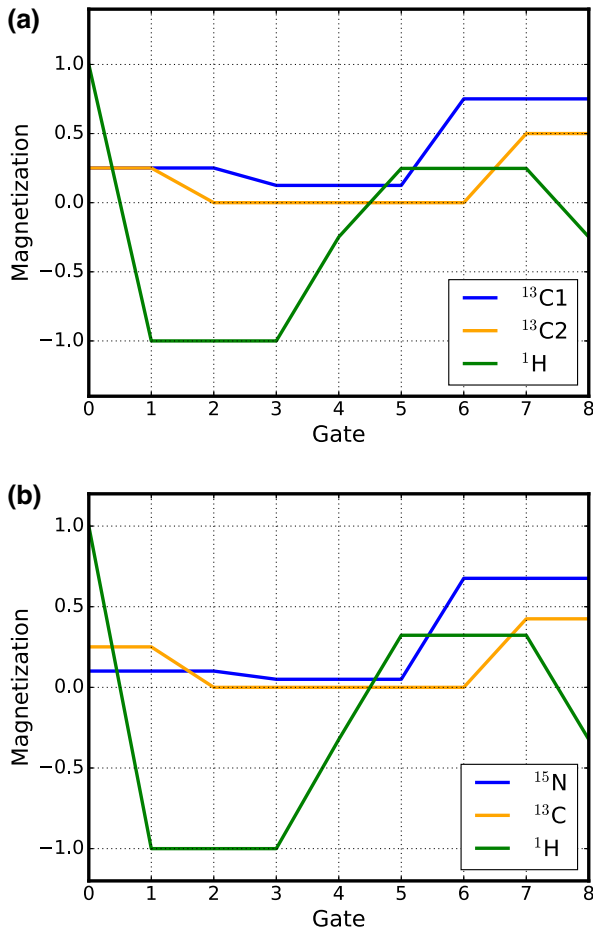| Spin	Initial polarization (ϵ_1)	Final polarization (ϵ_2)	T (K)
C1	0.25	1.075	70.46
C2	0.25	0.687	110.26
H	1	0.248	1221.77

FIG. 7. Plots of individual spin magnetizations after implementation of each quantum gate in the circuit of the compression unitary U_{TS} for the (a) $^{13}C_2$-labeled glycine system and the (b) ^{13}C-^{15}N-labeled formamide system. The gate number is indicated on the x axis.

CNOT, Toffoli, Toffoli, NOT, Toffoli, CNOT, and NOT gate, respectively [Fig. 2(a)]. The first three gates comprise the right shift operator, after implementation of which the entropy of the $^{13}C_1$ spin is decreased, that of the $^{13}C_2$ spin is maximized, and that of the ^1H spin remains the same. As seen from Fig. 7(a), the sixth gate, which is a Toffoli gate, has achieved entropy compression and complete increase of ^{13}C polarization. The subsequent gates manipulate the $^{13}C_2$ magnetization and invert the ^1H magnetization; the protocol could have been truncated at the seventh gate, which would have reduced the circuit complexity.

C. Experimentally cooling the ^{15}N spin

We were interested in exploring the efficiency of the TSAC algorithm on ^{15}N spins, due to their low initial polarizations at thermal equilibrium (approximately one-tenth that of the ^1H spin) as well as long T_1 relaxation

rates, which makes them attractive target spins for cooling. Hence, ^{15}N was chosen as the main target spin to be cooled in the ^{13}C-^{15}N-labeled formamide system and ^1H was chosen as the reset spin. This system also contains a ^{13}C spin which can also potentially be cooled down by the TSAC protocol. The reset spin relaxes much faster than the other spins and hence can be made to equilibrate quickly with the heat bath while the target spin remains relatively isolated from the heat bath.

1. Optimizing the TSAC reset delay

In order to optimize the reset delay at the end of the compression unitary implementation in the TSAC protocol, we simulated the change in ^{15}N spin polarization as a function of the reset delay. The TSAC reset delay was varied from $0.2T_1$ to $5T_1$ for the reset spin [Eq. (11)] and, as can be seen from Fig. 8, maximum ^{15}N polarization was obtained for a reset delay of approximately $2.5T_1$. We therefore set the value of the reset delay to this optimal value and performed multiple rounds of TSAC cooling.

2. Spin temperature after several TSAC cycles

The ^{15}N spectra at thermal equilibrium (plotted in red color) and after implementation of the TSAC cooling procedure (plotted in blue) are shown in Fig. 4(b). A substantial increase in polarization of the ^{15}N was achieved after TSAC cooling (approximately 5.95 times). As seen from the spectra in Fig. 4(b), the spectral peaks at the extreme positions in the thermal equilibrium spectra are barely visible, while after algorithmic cooling their signal-to-noise ratio has been significantly increased. The theoretical value of maximum achievable ^{15}N polarization (Shannon bound) for the ^{13}C-^{15}N-labeled formamide system computed from
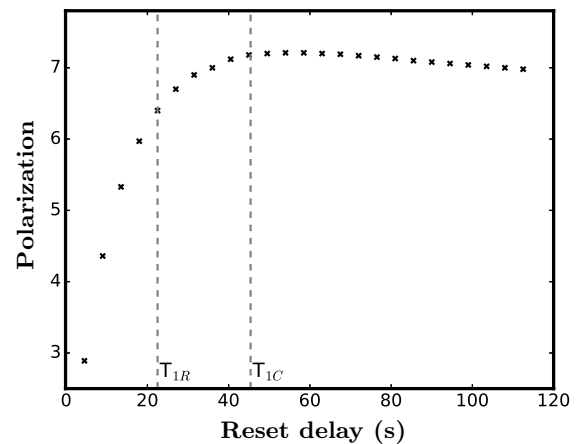

FIG. 8. Simulation of ^{15}N spin polarization as a function of the TSAC reset delay for the ^{13}C-^{15}N-labeled formamide system; T_{1R} and T_{1C} are the T_1 relaxation times of the ^1H reset spin and the ^{15}N computation spin, respectively.
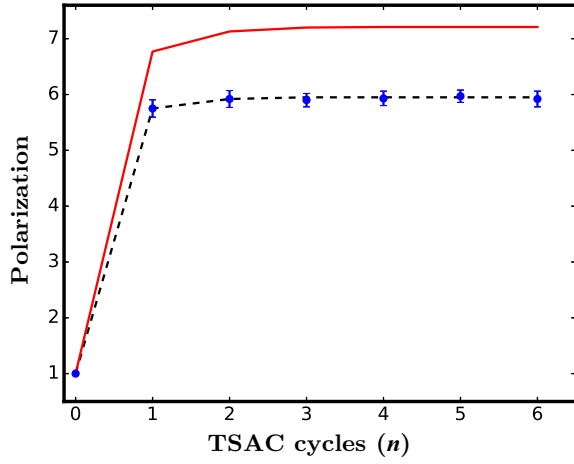
FIG. 9. Polarization of the ^{15}N spin versus number of cycles (n) of TSAC algorithmic cooling implemented on the ^{13}C-^{15}N-labeled formamide system. Theoretically expected and experimentally obtained values are depicted by a black dashed line and blue dots, respectively. The dotted line denotes the theoretical prediction of the polarization enhancement, taking into account the actual gate fidelities and reset delays. The red curve is the theoretically calculated polarization enhancement with ideal gate implementation for ^{13}C-^{15}N-labeled formamide system parameters.

Eq. (3) is given by

$$IC_{eq} = 104.56 \frac{\epsilon_{N, eq}^2}{\ln 4} = \frac{\epsilon_{SB}^2}{\ln 4} \qquad (13)$$
$$\Rightarrow \epsilon_{SB} = 10.22 \epsilon_{N,eq}.$$

After six rounds of TSAC cooling, we were able to experimentally achieve a final ^{15}N polarization of 0.595, and were not able to surpass the Shannon bound for this system. The final spin temperatures attained by all the three spins in the ^{13}C-^{15}N-labeled formamide system are tabulated in Table II. While the ^{15}N spin shows substantial cooling down to approximately 51 K, it is noteworthy that the ^{13}C spin has also been cooled down to approximately 187 K. The buildup of ^{15}N spin polarization after implementation of every cycle of TSAC cooling is shown in Fig. 9, and saturation of the polarization enhancement is attained after three cycles of TSAC cooling. The red curve in Fig. 9 is the theoretical prediction of the polarization with each round for ideal compression gate implementation. The black dotted curve depicts the polarization of the target qubit after taking into account the imperfections in the implementation of compression gate unitary. We observed that the compression unitary is implemented with an efficiency of 0.86 for the ^{13}C-^{15}N-labeled formamide system, which can be attributed to the magnetic field inhomogeneities, offset effects, and rf pulse miscalibrations.

TABLE II. Initial and final spin polarizations (ϵ_1, ϵ_2) and final spin temperature [T(K)] attained by each spin in the three-spin ^{13}C-^{15}N-labeled formamide system, after several rounds of algorithmic cooling. All polarization values are given relative to the initial polarization of the ^{1}H spin, which is set to 1.

Spin	Initial polarization (ϵ_1)	Final polarization (ϵ_2)	T (K)
N	0.101	0.595	51.43
C	0.251	0.406	187.32
H	1	-0.187	|1620.32|

3. Magnetization trajectories during compression unitary implementation

The plots of individual spin magnetizations of the ^{13}C-^{15}N-labeled formamide system at the end of the implementation of each quantum gate in the quantum circuit of the TSAC algorithm are shown in Fig. 7(b). The first three gates comprise the right shift operator, after implementation of which the entropy of the ^{15}N spin is decreased, that of the ^{13}C spin is maximized, and that of the ^{1}H spin remains the same. Hence, at this stage, the magnetizations of the ^{15}N, ^{13}C, and ^{1}H spins are halved, zeroed, and inverted, respectively. The sixth gate in the circuit, which is a Toffoli gate with control on the ^{1}H and ^{13}C spins and target on the ^{15}N spin, has decreased the entropy of the ^{15}N spin and correspondingly increased its polarization to its final experimental polarization. The final CNOT and NOT gates act to decrease the entropy of the ^{13}C spin and invert the magnetization of the ^{1}H spin.

In summary, the TSAC cooling protocol performs very well in cooling spins with low initial polarizations such as ^{13}C and ^{15}N spins. The protocol is robust and experimentally feasible. While maximum possible cooling was not achieved experimentally for the ^{15}N spin, this could be attributed to several factors including decoherence, rf inhomogeneities, and errors in the calibration of rf pulse parameters. The measured T_1 relaxation times (in seconds) of all the spins in the ^{13}C$_2$-labeled glycine system and in the ^{13}C-^{15}N-labeled formamide system are tabulated in Tables III and IV, respectively. The relaxation dynamics of the algorithmically cooled spins does not change appreciably after implementation of the TSAC protocol, implying that these systems retain their good dynamics properties, which are important for quantum computing. The gap

TABLE III. Measured relaxation times (in seconds) of all the spins in the three-spin ^{13}C$_2$-labeled glycine system, including the target spin at thermal equilibrium (C1^{hot}) and after algorithmic cooling (C1^{cold}).

	H	C2	C1^{hot}	C1^{cold}
T_1	1.57 ± 0.01	3.23 ± 0.03	20.4 ± 0.57	18.6 ± 0.4
T_2	1.0 ± 0.01	1.16 ± 0.02	1.53 ± 0.01	1.4 ± 0.01

TABLE IV. Measured relaxation times (in seconds) of all the spins in the three-spin ^{13}C-^{15}N-labeled formamide system, including the target spin at thermal equilibrium (N^{hot}) and after algorithmic cooling (N^{cold}).

	H	C	N^{hot}	N^{cold}
T_1	22.5 ± 0.675	30.40 ± 1.55	45.35 ± 2.25	50.67 ± 3.39
T_2	1.15 ± 0.16	1.33 ± 0.07	0.095 ± 0.009	0.115 ± 0.01

between the numerically computed upper bounds on the achievable polarizations for perfect TSAC conditions and the experimentally achieved polarizations suggests that cooling can be enhanced in systems with favorable relaxation properties by implementing several cycles of the TSAC protocol.

IV. CONCLUSIONS

While a major drawback of the standard PPA-HBAC protocol is that the operations for implementing compression are rather complex, change after every iteration, and hence require knowledge of the state in each iteration, other HBAC protocols have been developed which feature fixed rounds and are independent of the state of the system. An optimal HBAC protocol was recently designed, termed the TSAC method, which reaches the cooling limit using a fixed state-independent operation as the compression step. We used the TSAC method to purify selected target qubits in a system containing computational and reset qubits. We designed an optimal circuit decomposition of the compression unitary used in the protocol in terms of standard CNOT, Toffoli, and NOT gates which are experimentally viable to implement and which reduce the gate complexity of the TSAC method. Using an NMR quantum processor, we experimentally demonstrated the efficacy of the two-sort algorithmic cooling method in two different systems containing a target ^{13}C and ^{15}N spin. We obtained large polarization enhancements for both spins, which implies an appreciable decrease in the corresponding spin temperatures. We achieved significant cooling of the ^{15}N spin, with a polarization enhancement by a factor of approximately 5.95 which implies cooling down to a temperature approximately 51 K. Since ^{15}N has a very low polarization at room temperatures, our work has important implications for enhancing the signal-to-noise ratios, thereby reducing experimental acquisition times for 15N-labeled biomolecules such as peptides and proteins.

Since HBAC methods reduce the spin entropy and achieve spin cooling (and enhanced spin polarization) without the need for physical cooling of the system, they are safe and robust and have immense applications for *in vivo* NMR spectroscopy of slow metabolic processes. Our experimental implementation on an NMR quantum processor is intended to be a proof of principle of the TSAC method. However, the method is general and can be used to cool qubits in other quantum processing devices as well. We used this particular three-qubit NMR system for our experimental demonstration because of the relaxation properties of its work and reset qubits which satisfy the criteria for algorithmic cooling; however, the full advantage of the TSAC method will come into play for systems with more than three qubits, when the conventional PPA-HBAC method requires different unitaries in each round of cooling. Future work in this direction includes using the two-sort algorithm to enhance cooling of target qubits in larger-qubit registers of more than three qubits, and to investigate the performance of this algorithm and the attainable cooling limit in the presence of realistic noise.

The datasets generated during the current study are available from the corresponding author on reasonable request.

[1] M. A. Nielsen and I. L. Chuang, *Quantum Computation and Quantum Information* (Cambridge University Press, Cambridge, United Kingdom, 2010).

[2] Peter W. Shor, Polynomial-time algorithms for prime factorization and discrete logarithms on a quantum computer, SIAM J. Comput. **26**, 1484 (1997).

[3] Aram W. Harrow, Avinatan Hassidim, and Seth Lloyd, Quantum algorithm for linear systems of equations, Phys. Rev. Lett. **103**, 150502 (2009).

[4] Tian Wang, Roohollah Ghobadi, Sadegh Raeisi, and Christoph Simon, Precision requirements for observing macroscopic quantum effects, Phys. Rev. A **88**, 062114 (2013).

[5] John Preskill, Reliable quantum computers, Proc. R. Soc. A: Math. Phys. Eng. Sci. **454**, 385 (1998).

[6] D. G. Cory, R. Laflamme, E. Knill, L. Viola, T. F. Havel, N. Boulant, G. Boutis, E. Fortunato, S. Lloyd, R. Martinez,

C. Negrevergne, M. Pravia, Y. Sharf, G. Teklemariam, Y. S. Weinstein, and W. H. Zurek, NMR based quantum information processing: Achievements and prospects, Fortschritte der Phys. **48**, 875 (2000).

[7] L. M. K. Vandersypen and I. L. Chuang, NMR techniques for quantum control and computation, Rev. Mod. Phys. **76**, 1037 (2005).

[8] Kavita Dorai, T. S. Mahesh, and Arvind Anil Kumar, Quantum computation using NMR, Curr. Sci. **79**, 1447 (2000).

[9] David P. Divincenzo, The physical implementation of quantum computation, Fortschritte der Phys. **48**, 771 (2000).

[10] T. M. Cover and J. A. Thomas, *Elements of Information Theory* (Wiley-Interscience, Hoboken, New Jersey, USA, 2006).

[11] Noah Linden and Sandu Popescu, Good dynamics versus bad kinematics: Is entanglement needed for quantum computation? Phys. Rev. Lett. **87**, 047901 (2001).

[12] Leonard J. Schulman and Umesh V. Vazirani, in *Proceedings of the 31st annual ACM symposium on Theory of Computing* (ACM GA Atlanta USA, 1999), p. 322.

[13] P. Oscar Boykin, Tal Mor, Vwani Roychowdhury, Farrokh Vatan, and Rutger Vrijen, Algorithmic cooling and scalable NMR quantum computers, Proc. Natl. Acad. Sci. **99**, 3388 (2002).

[14] Phillip Kaye, Cooling algorithms based on the 3-bit majority, Quantum Inf. Process. **6**, 295 (2007).

[15] Algorithmic cooling of spins: A practicable method for increasing polarization, Int. J. Quantum Inf. **02**, 461 (2004).

[16] G. Brassard, Y. Elias, J. M. Fernandez, H. Gilboa, J. A. Jones, T. Mor, Y. Weinstein, and L. Xiao, Experimental heat-bath cooling of spins, Eur. Phys. J. Plus **129**, 266 (2014).

[17] Aaron Z. Goldberg and Khabat Heshami, Breaking the limits of purification: Postselection enhances heat-bath algorithmic cooling, J. Phys. Commun. **7**, 015003 (2023).

[18] Jan H. Ardenkjaer-Larsen, Bjorn Fridlund, Andreas Gram, Georg Hansson, Lennart Hansson, Mathilde H. Lerche, Rolf Servin, Mikkel Thaning, and Klaes Golman, Increase in signal-to-noise ratio of 10,000 times in liquid-state NMR, Proc. Natl. Acad. Sci. **100**, 10158 (2003).

[19] P. Bhattacharya, K. Harris, A. P. Lin, M. Mansson, V. A. Norton, W. H. Perman, D. P. Weitekamp, and B. D. Ross, Ultra-fast three dimensional imaging of hyperpolarized ^{13}C in vivo, MAGMA **18**, 245 (2005).

[20] Ana-Maria Oros and N. Jon Shah, Hyperpolarized xenon in NMR and MRI, Phys. Med. Biol. **49**, R105 (2004).

[21] J. M. Fernandez, Seth Lloyd, Tal Mor, and Vwani Roychowdhury, Algorithmic cooling of spins: A practicable method for increasing polarization, Int. J. Quantum Inf. **02**, 461 (2004).

[22] Leonard J. Schulman, Tal Mor, and Yossi Weinstein, Physical limits of heat-bath algorithmic cooling, SIAM J. Comput. **36**, 1729 (2007).

[23] Leonard J. Schulman, Tal Mor, and Yossi Weinstein, Physical limits of heat-bath algorithmic cooling, Phys. Rev. Lett. **94**, 120501 (2005).

[24] Yuval Elias, Tal Mor, and Yossi Weinstein, Semioptimal practicable algorithmic cooling, Phys. Rev. A **83**, 042340 (2011).

[25] Sadegh Raeisi and Michele Mosca, Asymptotic bound for heat-bath algorithmic cooling, Phys. Rev. Lett. **114**, 100404 (2015).

[26] Nayeli Azucena Rodríguez-Briones and Raymond Laflamme, Achievable polarization for heat-bath algorithmic cooling, Phys. Rev. Lett. **116**, 170501 (2016).

[27] Heat-bath algorithmic cooling with optimal thermalization strategies, Quantum **3**, 188 (2019).

[28] Sadegh Raeisi, No-go theorem behind the limit of the heat-bath algorithmic cooling, Phys. Rev. A **103**, 062424 (2021).

[29] Zahra Farahmand, Reyhaneh Aghaei Saem, and Sadegh Raeisi, Quantum noise can enhance algorithmic cooling, Phys. Rev. A **105**, 022418 (2022).

[30] J. Baugh, O. Moussa, C. A. Ryan, A. Nayak, and R. Laflamme, Experimental implementation of heat-bath algorithmic cooling using solid-state nuclear magnetic resonance, Nature **438**, 470 (2005).

[31] J. M. Fernandez, T. Mor, and Y. Weinstein, Paramagnetic materials and practical algorithmic cooling for NMR quantum computing, Int. J. Quantum Inf. **03**, 281 (2005).

[32] Y. Elias, H. Gilboa, T. Mor, and Y. Weinstein, Heat-bath cooling of spins in two amino acids, Chem. Phys. Lett. **517**, 126 (2011).

[33] Yosi Atia, Yuval Elias, Tal Mor, and Yossi Weinstein, Algorithmic cooling in liquid-state nuclear magnetic resonance, Phys. Rev. A **93**, 012325 (2016).

[34] Varad R. Pande, Gaurav Bhole, Deepak Khurana, and T. S. Mahesh, Strong algorithmic cooling in large star-topology quantum registers, Phys. Rev. A **96**, 012330 (2017).

[35] Daniel K. Park, Guanru Feng, Robabeh Rahimi, Stéphane Labruyère, Taiki Shibata, Shigeaki Nakazawa, Kazunobu Sato, Takeji Takui, Raymond Laflamme, and Jonathan Baugh, Hyperfine spin qubits in irradiated malonic acid: Heat-bath algorithmic cooling, Quantum Inf. Process. **14**, 2435 (2015).

[36] Daniel K. Park, Nayeli A. Rodriguez-Briones, Guanru Feng, Robabeh Rahimi, Jonathan Baugh, and Raymond Laflamme, in *Electron Spin Resonance (ESR) Based Quantum Computing* (Springer New York, New York, NY, 2016), p. 227.

[37] Nayeli A. Rodríguez-Briones, Eduardo Martín-Martínez, Achim Kempf, and Raymond Laflamme, Correlation-enhanced algorithmic cooling, Phys. Rev. Lett. **119**, 050502 (2017).

[38] Raymond Laflamme, Junan Lin, and Tal Mor, Algorithmic cooling for resolving state preparation and measurement errors in quantum computing, Phys. Rev. A **106**, 012439 (2022).

[39] C. A. Ryan, O. Moussa, J. Baugh, and R. Laflamme, Spin based heat engine: Demonstration of multiple rounds of algorithmic cooling, Phys. Rev. Lett. **100**, 140501 (2008).

[40] Emre Köse, Sel çuk Çakmak, Azmi Gençten, Iannis K. Kominis, and Özgür E. Müstecaplıoğlu, Algorithmic quantum heat engines, Phys. Rev. E **100**, 012109 (2019).

[41] Nayeli A. Rodríguez-Briones, Jun Li, Xinhua Peng, Tal Mor, Yossi Weinstein, and Raymond Laflamme, Heat-bath algorithmic cooling with correlated qubit-environment interactions, New J. Phys. **19**, 113047 (2017).

[42] Sebastian Zaiser, Chun Tung Cheung, Sen Yang, Durga Bhaktavatsala Rao Dasari, Sadegh Raeisi, and Jörg Wrachtrup, Cyclic cooling of quantum systems at the saturation limit, npj Quantum Inf. 7, 92 (2021).

[43] Rodolfo R. Soldati, Durga B. R. Dasari, Jörg Wrachtrup, and Eric Lutz, Thermodynamics of a minimal algorithmic cooling refrigerator, Phys. Rev. Lett. **129,** 030601 (2022).

[44] Sadegh Raeisi, Mária Kieferová, and Michele Mosca, Novel technique for robust optimal algorithmic cooling, Phys. Rev. Lett. **122,** 220501 (2019).

[45] Kavita Dorai and Dieter Suter, Efficient implementations of the quantum fourier transform: An experimental perspective, Int. J. Quantum Inf. **03,** 413 (2005).

[46] Ole Winneche Sørensen, Polarization transfer experiments in high-resolution NMR spectroscopy, Prog. Nucl. Magn. Reson. Spectrosc. **21,** 503 (1989).

[47] Adriano Barenco, Charles H. Bennett, Richard Cleve, David P. DiVincenzo, Norman Margolus, Peter Shor, Tycho Sleator, John A. Smolin, and Harald Weinfurter, Elementary gates for quantum computation, Phys. Rev. A **52,** 3457 (1995).

[48] I. S. Oliveira, T. J. Bonagamba, R. S. Sarthour, J. C. C. Freitas, and E. R. deAzevedo, *NMR Quantum Information Processing* (Elsevier Science B.V., Amsterdam, 2007).

[49] Debmalya Das, Shruti Dogra, Kavita Dorai, and Arvind, Experimental construction of a w superposition state and its equivalence to the Greenberger-Horne-Zeilinger state under local filtration, Phys. Rev. A **92,** 022307 (2015).

[50] Harpreet Singh, Arvind, and Kavita Dorai, Evolution of tripartite entangled states in a decohering environment and their experimental protection using dynamical decoupling, Phys. Rev. A **97,** 022302 (2018).

[51] Amandeep Singh, Harpreet Singh, Kavita Dorai, and Arvind, Experimental classification of entanglement in arbitrary three-qubit pure states on an NMR quantum information processor, Phys. Rev. A **98,** 032301 (2018).